1   **Effects of seawater pCO$_2$ on the skeletal morphology of massive Porites spp. corals.**

2

3   Nicola Allison[*1], Phoebe Ross[1a], Alex Brasier[2], Nadia Cieminska[1], Nicolas Lopez Martin[1], Catherine

4   Cole[1b], Chris Hintz[3], Ken Hintz[4], Adrian Finch[1]

     *Corresponding author, email: na9@st-andrews.ac.uk, ORCID 0000-0003-3720-1917

5

6   [1]School of Earth and Environmental Sciences, University of St. Andrews, St. Andrews KY16 9AL,

7   UK

8   [2] School of Geosciences, Meston Building, University of Aberdeen, AB24 3UE

9   [3] Department of Marine and Environmental Sciences, Savannah State University, Savannah, GA

10   USA

11   [4] Department of Electrical and Computer Engineering, George Mason University, Fairfax, VA, USA

12

13   [a] Now at Department of Earth Science and Engineering, Imperial College London, London, UK

14   [b] Now at Department of Science Communication, University of Otago, Dunedin, 9016, New

15   Zealand.

16

17   Keywords: coral, calcification, skeleton, polyp size, ocean acidification

18

19   **<u>Abstract</u>**

20   Ocean acidification alters the dissolved inorganic carbon chemistry of seawater and can

21   reduce the calcification rates of tropical corals. Here we explore the effect of altering seawater

22   pCO$_2$ on the skeletal morphology of 4 genotypes of massive *Porites* spp which display widely

23   different calcification rates. Increasing seawater pCO$_2$ causes significant changes in in the skeletal

24   morphology of all *Porites* spp. studied regardless of whether or not calcification was significantly

25   affected by seawater pCO$_2$. Both the median calyx size and the proportion of skeletal surface

26   occupied by the calices decreased significantly at 750 μatm compared to 400 μatm indicating that

27   polyp size shrinks in this genus in response to ocean acidification. The coenosteum, connecting

28   calices, expands to occupy a larger proportion of the coral surface to compensate for this decrease

29   in calyx area. At high seawater pCO$_2$ the spines deposited at the skeletal surface became more

30   numerous and the trabeculae (vertical skeletal pillars) became significantly thinner in 2 of the 4

31   genotypes. The effect of high seawater pCO$_2$ is most pronounced in the fastest growing coral and

32   the regular placement of trabeculae and synapticulae is disturbed in this genotype resulting in a

33   skeleton that is more randomly organised. The study demonstrates that ocean acidification

34   decreases the polyp size and fundamentally alters the architecture of the skeleton in this major reef

35   building species in the Indo-Pacific Ocean.

36

Introduction

37

38   Tropical corals produce the skeletons that underpin coral reef structures and provide

39   habitat spaces for a diverse range of biota. In 2015 the value of tropical coral reefs as resources

40   for fisheries, tourism and land protection was estimated to exceed US$30 billion annually (Chen,

41   2015). Increasing atmospheric CO_2 is altering the chemistry of seawater, decreasing ocean pH

42   (IPCC 2019) and reducing the calcification of many tropical corals (Erez et al., 2011). Corals build

43   the skeleton at calcification sites which are isolated from seawater either from media contained

44   between the coral tissue and the skeleton (Allemand et al., 2011) or in intracellular vesicles (Drake

45   et al., 2018). The coral increases the pH of the calcification media above that of seawater (Al

46   Horani et al., 2003, Venn et. al. 2011). This shifts the dissolved inorganic carbon equilibrium to

47   increase CO_3^{2-}, one of the substrates for $CaCO_3$ formation, and likely promotes calcification.

48   However, in corals cultured under high seawater pCO_2, the pH of the calcification media is lower

49   than in corals cultured at lower pCO_2 (Venn et al., 2013, Allison et al., 2021) and this likely

50   decreases the proportion of DIC present as $[CO_3^{2-}]$.

51   Coral skeletons are organic:inorganic composites composed of the mineral aragonite and

52   biomolecules e.g. proteins and polysaccharides, secreted by the coral (Falini et al., 2015). The

53   concentration of the skeletal organic matrix and its constituents has been observed to increase in

54   response to rising seawater pCO_2 (Tambutte et al., 2015, Coronado et al., 2019, Kellock et al.,

55   2020). $CaCO_3$ precipitation can be promoted and inhibited by biomolecules (Elhadj et al., 2006)

56   and the organic matrix extracted from biogenic calcareous structures can influence both the

57   morphology of $CaCO_3$ crystals precipitated *in vitro* (Falini et al., 2013) and their physical properties

58   (Herman et al., 1988, Kim et al., 2016). Alterations in the concentration or composition of the

59   skeletal organic matrix may account for the changes in coral skeletal architecture which can be

60   observed in response to high seawater pCO_2 e.g. increases in calyx size (Tambutte et al., 2015),

61   variations in crystal appearance (Coronado et al., 2019) and decreases in the abundance of the

62   rapid accretion deposits on the skeletal surface (Scucchia et al., 2021).

63   In this study we investigated the effect of changes in seawater pCO_2 on the skeletal

64   morphology of cultured massive *Porites* spp. Massive *Porites* spp. can be important contributors to

65   reef building in the Indo-Pacific (Veron 1993) and may be relatively resilient to rising seawater

66   pCO_2. *Porites* spp. persist at naturally high pCO_2 reef sites (Fabricius et al., 2011; Crook et al.,

67   2012) and may even increase their coverage compared to adjacent lower pCO_2 control sites

68   (Fabricius et al., 2011). The calcification, photosynthesis and respiration rates of the corals

69   examined in the current study were reported by Cole et al. 2018. Increasing seawater pCO_2

70   decreased calcification significantly in some *Porites* spp. individuals but not in others (Cole et al.,

71   2018). This contrasts with a study of juvenile Porites which found no significant effect of seawater

72   pCO_2 on calcification (Edmunds 2012). For the present study we compare the sizes of key skeletal

73   features (calyx size and trabecula width) between seawater pCO_2 treatments and explore the

74   skeletal morphology by scanning electron microscopy. We examine 2 *Porites* species (*P. lutea* and

75 _P. murrayensis_) and include different individuals which either exhibited reduced calcification rates
76 at high seawater pCO_2 or appeared unaffected (Cole et al., 2018).

77

78 **Methods and materials**

79 **Coral culturing**

80   We cultured massive _Porites_ spp. corals over a range of seawater pCO_2 (~180, 400 and
81 750 µatm) in two experiments, previously described (Cole et al., 2016, 2018). Full details of the
82 methodology and seawater chemistry are provided in Appendix A. These pCO_2 reflect conditions in
83 the Last Glacial Maximum, the present day and a potential future CO_2 scenario (Barry et al., 2011).
84 In the first experiment corals were maintained at target pCO_2 and 25°C for 6-7 months before
85 sacrifice. In the second experiment corals were maintained at target pCO_2 and 28°C for 5-6
86 months before the temperature was decreased to 25°C over a period of one month and then the
87 corals held at this temperature for 9 weeks before sacrifice. For each experiment we sawed
88 imported coral heads into multiple pieces (each ~12 cm in diameter) so that at least one large
89 piece of each head could be cultured in each seawater pCO_2 treatment. The corals were
90 considered to represent different genotypes when they were collected from spatially separate (non-
91 adjoining) colonies. Although the temperature regimes vary between the two experiments we
92 compare variations in skeletal morphology within each coral genotype. All coral skeletons were
93 cleaned with sodium hypochlorite and rinsed and dried before analysis. We examined the skeletal
94 morphology of 4 genotypes (numbered 1, 4, 6 and 7, following the convention used in Cole et al.,
95 2018). Genotypes 1 and 7 were identified as _P. lutea_ and genotypes 4 and 6 were identified as _P._
96 _murrayensis_ on the basis of corallite structure (Veron 1993). In 2 genotypes (4 and 7) calcification
97 was significantly reduced at 750 µatm pCO_2 compared to 180 µatm while in the other 2 genotypes
98 (1 and 6) calcification rate differences were not significant (Cole et al. 2018).

99   Samples with a surface area of 1-3 cm^2 were cut from the surface of each skeleton using a
100 handheld circular saw, cleaned in an ultrasonic bath and dried before imaging of the skeletal
101 surface. Cross section samples through the coral skeleton were prepared by cutting a slice through
102 the centre of the coral heads and then cutting a strip of skeleton about 10 mm wide along the
103 maximum growth axis of the slice. The outermost 1.5 cm on the strips were fixed in 25 mm circular
104 epoxy resin blocks (Epofix, Struers Ltd.), polished with silicon carbide papers and alumina (Allison
105 et al., 2021) and photographed under reflected light microscopy.

106

107 **Corallite measurements**

108   The skeleton surfaces were photographed using a Keyence VHX-2000E digital microscope.
109 The focus-stacking function was used to create in-focus images of the three dimensional surface
110 with each image recording an area of 5.2 x 6.9 mm. We recorded 4 or more images of each coral
111 skeleton, focusing on areas at the centre of each skeleton, where growth rate was maximal and
112 avoiding depressions where corallites were growing towards each other.

3

The key skeletal structures examined in this study are illustrated in Figure 1. *Porites* spp. corals are colonial and composed of multiple polyps. The skeleton deposited by each polyp is called a corallite (Figure 1a). At the centre of each corallite is a calyx (plural calices), an approximately circular cup that houses the polyp. Vertical partitions called septae radiate from the corallite wall towards the centre of the calyx. At the centre of the corallite, extensions of the septae may intertwine to form a columella, a structure present in some *Porites* species e.g. *P. lutea* but absent in others e.g. *P. murrayensis*. Individual calices are joined by the coenosteum, the skeleton deposited between polyps. In this study we determined the surface area of the coral calices at the surface of the skeleton and calculated the % of surface area that was occupied by polyps (in contrast to coenosteum).
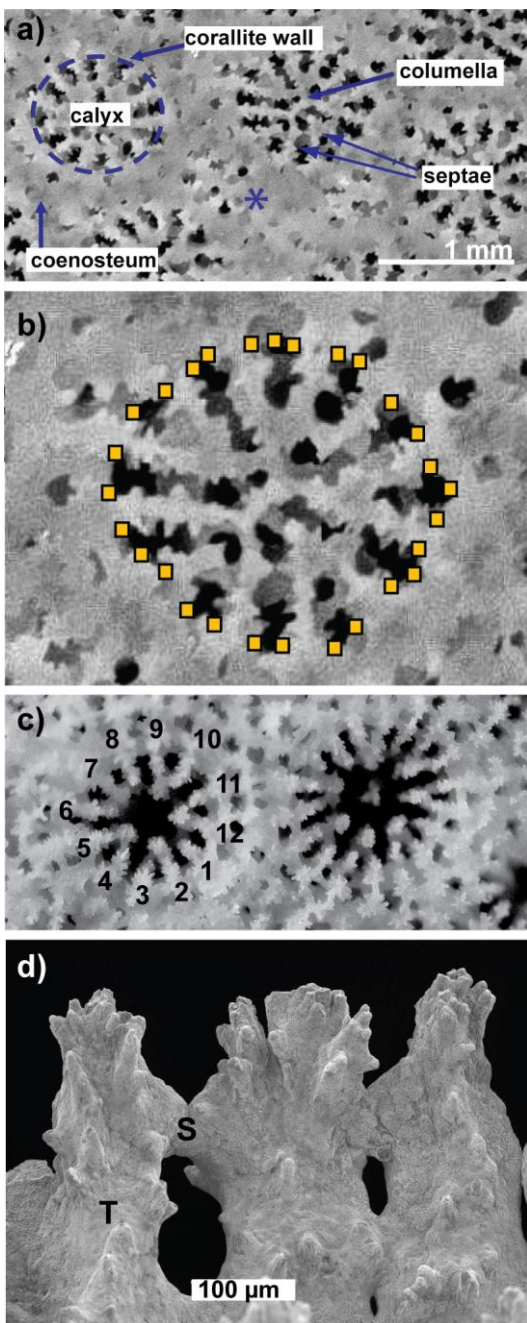
Figure 1. Photomicrographs of a) a *P. lutea* skeleton with key skeletal structures annotated, * marks a new polyp forming by extratentacular budding, b) positions of line segments in ImageJ to estimate calyx area in a typical corallite and c) surface of a *P. murrayensis* specimen. Twelve septae are typically visible in each corallite (see numbers on left hand polyp) but in some relatively large corallites more septae are visible (right hand polyp) suggestive of polyp division by intratentacular budding. d) Skeletal trabeculae (T) and synapticulae (S) at the very surface of the skeleton.

4

124   The area of each calyx in each image was measured on scaled photographs using the
125   image processing software, ImageJ (National Institute of Health, USA). Using the polygon selection
126   tool we create line segments along the internal edge of the corallite wall and at the intersection of
127   septa and the corallite wall (Figure 1b). The software interpolated between these segments and
128   calculated the calyx surface area. We combined the measurements of all whole calices i.e. where
129   the photograph recorded the whole calyx and did not cut off part of the structure, to determine the
130   size distribution of polyps in the coral. For each image the area of all calices in the image (both
131   whole and partial corallites) was summed and divided by the total surface area of the image to
132   each provide an estimate of the percentage of the skeletal surface occupied by polyps (compared
133   to the coenosarc tissue interconnecting the polyps). We explored the impact of seawater pCO_2 on
134   calyx sizes and calyx:coenosteum ratio in the different coral genotypes. The entire skeleton is
135   composed of vertical pillars, called trabeculae, which are interconnected by horizontal rungs, called
136   synapticulae (Figure 1d). We used the cross section photographs to measure the widths of the
137   trabeculae in each coral at a depth of 1 mm from the coral surface. Calcification rates varied from 4
138   to 35 µmol cm^{-2} day^{-1} at 25°C in the corals examined here (Cole et al., 2018) so this position in the
139   skeleton represents a different time point in each coral. We measured trabecula widths at this
140   position to ensure we compared comparable spatial positions in the skeleton.
141

Scanning electron microscopy

143   Scanning electron micrograph images were collected for genotypes 4, 6 and 7. Skeletal
144   samples were mounted on aluminium pin stubs (25 mm diameter) using double-sided carbon
145   adhesive discs. Samples were double carbon-coated under vacuum (Quorum K950 carbon
146   coater), rotating the samples 90° between coats to ensure full coverage. Samples were viewed
147   using a CarlZeiss GeminiSEM 300 (ACEMAC Facility, University of Aberdeen) using an
148   accelerating voltage of 5keV and an SE2 detector for the lowest magnification images, and 1.5 keV
149   and an InLens secondary electron detector for all other magnifications.
150

Results

Corallite measurements

153   Sample photomicrographs showing the calyx sizes of coral genotype 1 cultured over
154   varying seawater pCO_2 and the calyx size distributions of all corals are summarised in Figure 2.
155   Similar photomicrographs of all coral individuals are included in the supplementary information.
156   The populations of calyx size within each coral are not normally distributed (Shapiro Wilk test). The
157   *P. lutea* corals exhibit size distributions with a negative skew i.e. most corallites had a narrow
158   range of large calyx surface areas but there is usually a tail of smaller calices (Figure 2b). The *P.*
159   *murrayensis* corals exhibit size distributions that are more symmetrical with tails of both small and
160   large calices. Colonial corals enlarge by budding, where parent polyps divide to produce 2 or more
161   daughter polyps. Budding can occur outside the polyp tentacle ring (extratentacular), resulting in

5

the daughter polyp forming on the side of the parent polyp, or can be intratentacular, resulting in the division of the parent corallite into 2 or more corallites (Veron, 1986). In the *P. lutea* skeletons we observe evidence of extratentacular budding (Figure 1a) in all seawater pCO_2 treatments. Small corallites form on the skeletal surface adjacent to parent polyps that are similar in size to their non-budding counterparts. Extratentacular budding generates small polyps that gradually get bigger and this explains the negative skew observed in the *P. lutea* calyx size distributions. In the *P. murrayensis* skeletons budding appears to be largely intratentacular (Figure 1c). We observe relatively large corallites which contain more septae than the usual 12 and we infer that these represent polyps in the process of division. Intratentacular budding generates both large and small polyps as the dividing polyp first enlarges and then splits into 2 smaller individuals, explaining the tails of larger and smaller calices observed in the size distributions of this species. We observe intratentacular budding in all seawater pCO_2 treatments.

Figure 2. a) Photomicrographs of the skeleton surface of genotype 1 grown at contrasting seawater pCO_2 and b) calyx size distributions in all genotypes.
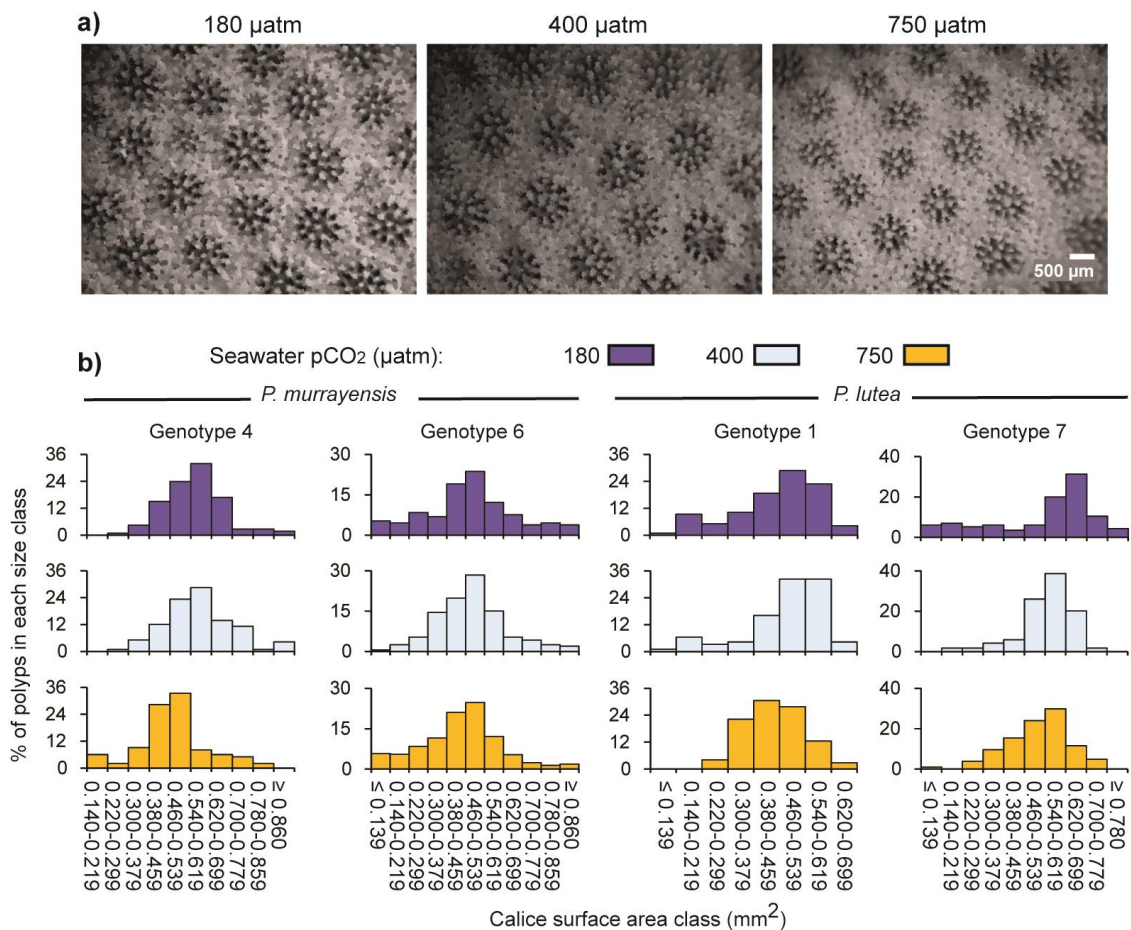
180   We compared the size distributions between seawater pCO_2 treatments within each coral

181 genotype using the Kolmogorov–Smirnov test (Table 1). The calyx size distributions are

182 significantly different ($p<0.05$) between corals cultured at 750 and 400 µatm for each coral

183 genotype but are only significantly different between 180 and 400 µatm for genotype 1. The mode

184 (most common) calyx size class is smaller in corals cultured at 750 µatm compared to 180 µatm in

185 3 of the 4 genotypes (1, 4 and 7) and compared to 400 µatm in 2 of the 4 genotypes (1 and 4,

186 Figure 2b). The mean and median (the middle value in the dataset) calyx surface areas were

187 always smaller in corals cultured at 750 µatm compared to 400 µatm (Table 2). The Kruskal Wallis

188 test for equal medians indicates that medians are significantly different between corals cultured at

189 750 µatm compared to 400 µatm for all genotypes (Table 1).

190   To test for the normality of distribution in our estimates of the proportion of calyx surface

191 area as a % of total skeletal surface we photographed and analysed additional images of the

192 surfaces of the genotype 6 coral cultured at 400 and 750 µatm (12 and 22 images respectively).

193 These populations are normally distributed (Shapiro Wilk test) and we compare the proportion of

194 calyx surface area as a % of total skeletal surface between seawater pCO_2 treatments within each

195 genotype using one way ANOVA. The % of the skeletal surface as calyx was significantly lower at

196 750 µatm compared to 400 µatm in all genotypes and significantly higher at 180 µatm compared to

197 400 µatm in just one genotype, G7 (Table 1, Figure 3a).

198

199 **Table 1**. Summary of p values for statistical tests comparing calyx surface area median (Kruskall

200 Wallis), calyx size distribution (Kolmogorov–Smirnov), % of skeletal surface as calyx (ANOVA) and

201 trabeculae width (ANOVA) between individuals of the same genotype cultured under different

202 seawater pCO_2. p values ≤ 0.05 are highlighted in bold.

Genotype	Calyx surface area median		Calyx size distribution		Calyx area as % of surface		Trabecula width	
	180 v 400	400 v 750	180 v 400	400 v 750	180 v 400	400 v 750	180 v 400	400 v 750
1	**0.024**	**6.6×10^{-4}**	0.081	**1.1×10^{-3}**	0.25	**0.022**	**0.019**	0.48
4	0.33	**2.3×10^{-8}**	0.15	**1.5×10^{-8}**	0.15	**1.7×10^{-3}**	1.0	**0.021**
6	0.82	**1.1×10^{-4}**	0.16	**1.3×10^{-3}**	0.29	**0.041**	1.0	0.36
7	0.19	**0.033**	**2.7×10^{-4}**	**3.1×10^{-3}**	**3.6×10^{-3}**	**7.2×10^{-5}**	0.64	**6.0×10^{-4}**

203

204 **Table 2**. Mean ($\pm 1\sigma$) and median calyx surface areas (mm^2) in each coral genotype at each

205 seawater pCO_2 treatment. n is shown in parentheses in the median side of the table.

	Mean			Median		
	180 µatm	400 µatm	750 µatm	180 µatm	400 µatm	750 µatm
Genotype 1	0.45 ± 0.13	0.48 ± 0.12	0.44 ± 0.09	0.49 (118)	0.52 (93)	0.45 (72)
Genotype 4	0.56 ± 0.14	0.58 ± 0.14	0.47 ± 0.14	0.56 (113)	0.56 (116)	0.47 (99)
Genotype 6	0.48 ± 0.19	0.45 ± 0.15	0.44 ± 0.17	0.49 (131)	0.48 (359)	0.45 (712)
Genotype 7	0.53 ± 0.20	0.55 ± 0.10	0.51 ± 0.12	0.60 (116)	0.56 (119)	0.52 (104)

Figure 3. Variations in a) % of skeletal surface area occupied by calices (in contrast to coenosteum) in each coral and b) mean trabecula width in each coral. c) For comparison the calcification data for each coral at 25°C is replotted from Cole et al., 2018. Error bars in each case are 95% confidence limits.

206
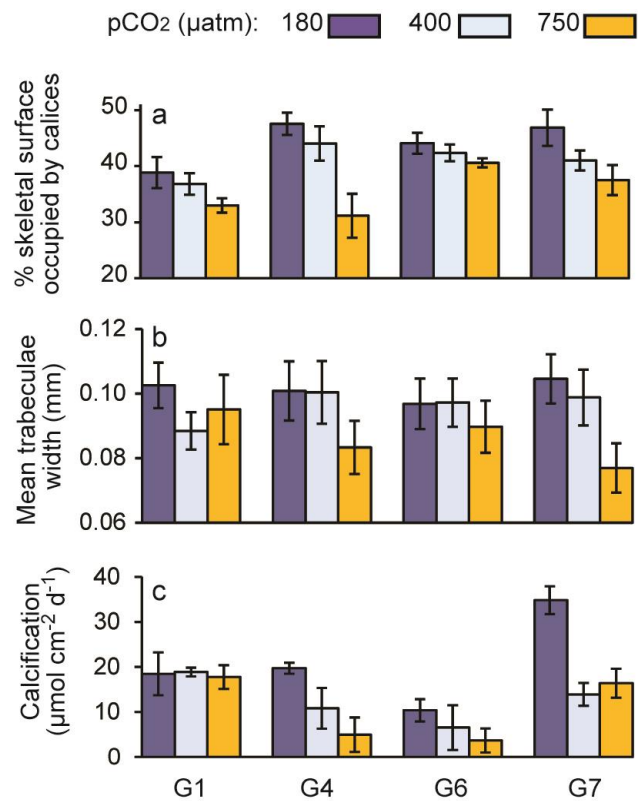
Mean trabecula width

208   *Porites* spp. produce perforate skeletons and both the septae and coenosteum are
209 composed of vertical trabeculae interconnected with horizontal synapticulae (Figure 1d). These
210 units are typically deposited at approximate right angles to each other and at approximately regular
211 intervals resulting in an interconnecting structure with pore spaces that appear circular or oval
212 (Figure 4a). Sample light micrographs of trabecula and synapticulae in each coral are in the
213 supplementary information. We measured the width of the trabecula at a distance of 1 mm from the
214 coral surface in each coral. Trabeculae are significantly narrower in the genotype 4 and 7 corals
215 cultured at 750 µatm compared to the corals cultured at 400 µatm (Figure 3b, Table 1) and in the
216 genotype 1 coral cultured at 400 µatm compared to 180 µatm. Other differences are not significant.
217 The regular placement of trabecula and synapticulae is disturbed in genotype 7 cultured at 750
218 µatm and the connections between structures become more randomly organised (Figure 4b).
219
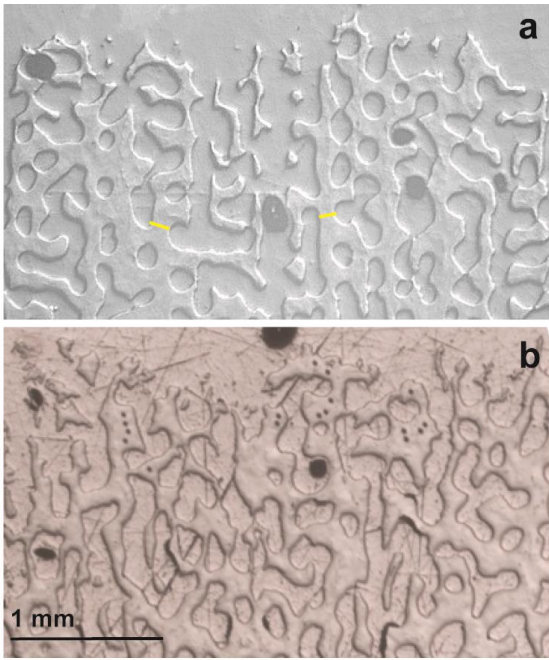
Figure 4. Reflected light micrographs of cross-sections through the outermost surface of coral genotype 7 cultured at a) 400 µatm and b) 750 µatm. Typical positions of trabeculae width measurements are shown by yellow lines. Ion microprobe analysis pits are visible as small black dots on the images.
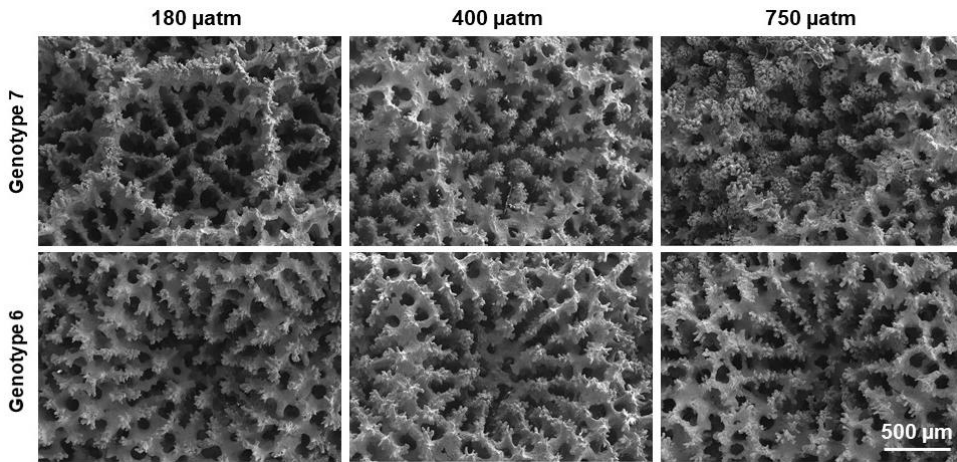
Scanning electron microscopy

Sample scanning electron micrographs of the corallite structure and skeletal surface are shown in Figures 5 and 6. Additional images of each coral are included in the supplementary data. At the surface of the *Porites* spp. skeleton the extending trabeculae terminate in projections or spines which can appear as fingers radiating from a hand (Figure 1d) and are typically 10-30 µm in height and width. The spines become noticeably more abundant at high seawater pCO_2 resulting in skeletons which appear more ornate (Figures 5 and 6). This effect was least apparent in genotype 6 and most pronounced in genotype 7 (Figure 6). We did not observe consistent changes in the appearance of the skeletal surface at the micron scale in response to seawater pCO_2 (Figure 6).

Figure 5. Scanning electron micrographs (secondary electron images) of corallites of 2 coral
233 genotypes cultured over a range of seawater pCO_2.
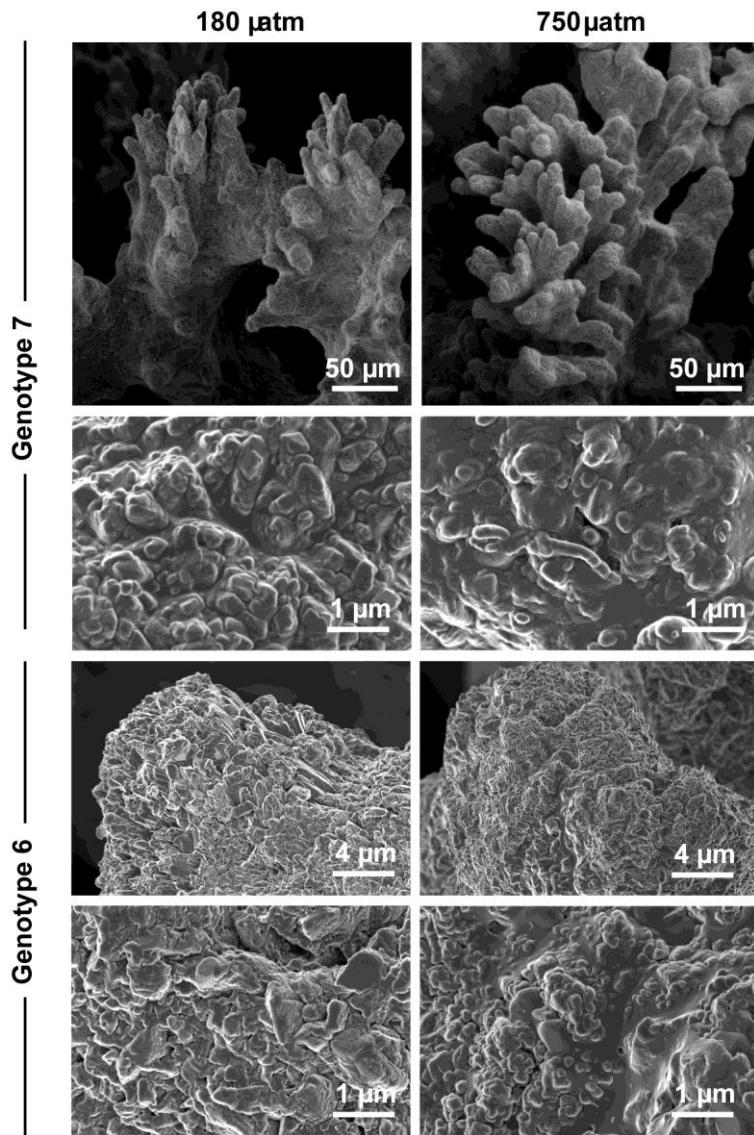
234

235
236
237

Figure 6. Scanning electron micrographs of the skeleton surface of coral genotype 7 and 6 grown at contrasting seawater pCO_2. Images show the ends of trabeculae in the corallite wall (50 μm scale bar) and the skeletal surface at the micron scale (other images).

238

Discussion

Impacts of seawater pCO$_2$ on skeletal morphology

Our study shows that increasing seawater pCO$_2$ causes significant changes in in the skeletal morphology of massive Porites spp. corals. These changes were observed in all *Porites* spp. genotypes regardless of whether or not calcification was significantly affected by seawater pCO$_2$. Our study indicates that coral polyps likely become smaller in *Porites* spp. cultured at high seawater pCO$_2$ compared to present day values. Both the median calyx size and the proportion of skeletal surface occupied by the calices decreases significantly at 750 µatm compared to 400 µatm (Table 1). The coenosteum, connecting calices, expands to occupy a larger proportion of the coral surface at high seawater pCO$_2$ indicating that the coenosarc, the tissue connecting polyps, increases in area. On average, over all genotypes, mean and median calyx areas are reduced by 9 and 10% respectively at 750 µatm compared to 400 µatm. High seawater pCO$_2$ decreased corallite height in *Siderastrea siderea* by 10-15% (Horvath et al., 2016) which would have resulted in a reduction in polyp volume of the order observed in this study. Decreasing seawater pCO$_2$ below the modern value had little significant impact on skeletal morphology in this study. The median calyx surface was smaller, but the trabeculae were wider in the G1 corals cultured at 180 µatm compared to 400 µatm while the proportion of skeleton occupied by calices increased in the G7 corals cultured at 180 µatm.

Our finding contrasts with other coral studies which find that calyx size increases at high seawater pCO$_2$ (Tambutte et al., 2015) or remains constant (Scucchia et al., 2021) and that coenosteum area decreases (Scucchia et al., 2021a). The rate at which corals produce CaCO$_3$ is often reduced at high seawater pCO$_2$ (Erez et al., 2011) and calcification rates were significantly lower in individuals of genotype 4 and 7 (but not genotypes 1 and 6) grown at 750 µatm compared to 180 µatm in the specimens examined in this study (Cole et al., 2018). Increases in calyx size are one route that corals may take to reduce the amount of CaCO$_3$ required to build the skeletons. However, increasing calyx size requires that the polyp volume (occupying the calyx) also increases and this likely involves an energetic cost in increasing tissue biomass. We know of no other reports of reductions in polyp/calyx size in response to increasing seawater pCO$_2$ but heat stress is associated with a decrease in body size in polyps of Mediterranean sea anemones (Chomsky et al., 2004) and in corallites of modern solitary corals (Kersting and Linares, 2019). Lasker (1981) reported a decrease in the ratio of polyp area:coenosarc area in *Montastrea cavernosa* growing at depth compared to shallow water individuals and hypothesised that this morphological adaption reduced colony maintenance costs.

Polyps in two colonial coral species (*Pocillopora damicornis* and *Oculina patagonia*) ultimately dissociated from the coenosarc under extreme pH conditions (Kvitt et al.,2015) and the reduction in polyp size suggested by our study may be a first step in this process. Although it is unclear if the reductions in calice areas observed in this study reflect a decrease in the polyp size or a reduction in CaCO$_3$ deposition, these changes in the ratio of polyp:coenosarc area likely have

277 implications for the function of the coral. For example, the photosynthetic activities of coenosarc
278 tissues are lower than in adjacent polyps in *Pocillopora damicornis* (Ulstrup et al., 2006) and
279 reducing the polyp area:coenosarc area ratio of colonies may decrease the colony primary
280 production.

281   Our observation of a significant narrowing of the width of the skeletal trabecula in two of the
282 coral genotypes (G4 and G7) at high seawater pCO_2 agrees with other studies which report a
283 thinning of skeletal structures under ocean acidification conditions (Tambutte et al., 2015; Scucchia
284 et al., 2021a). Skeletal density but not linear extension correlates positively with seawater
285 saturation state (Ω) in *Porites* spp. collected from multiple reefs sites spanning a range of Ω
286 (Mollica et al., 2018) suggesting that reduced calcification in *Porites* spp in response to high
287 seawater pCO_2 decreases skeletal density but not linear extension. Reducing the thickness of
288 skeletal units and increasing macro- and micro- skeletal porosity (Horvath et al., 2016; Foster et
289 al.; 2016, Tambutte et al., 2015) all act to decrease skeletal density.

290   The numbers of spines formed on the skeletal growth surface of the *Porites* spp. increases
291 at high seawater pCO_2 (Figures 5 and 6). These spines are the first structures to develop as the
292 coral extends its skeleton and likely form by the attachment of amorphous calcium carbonate
293 (ACC) nanoparticles in an organic rich matrix. These transform to crystalline aragonite producing
294 features a few microns in diameter (Drake et al., 2020). The features are termed rapid accretion
295 deposits (RADs) and are also known as centres of calcification (Wells, 1956) and early
296 mineralisation zones (Cuif and Dauphin, 2005). Aragonite fibres radiate out from the RADs to
297 produce bundles of acicular crystals called thickening deposits (TD) which make up the bulk of the
298 trabeculae. Coronado et al. (2019) observed a pronounced lengthening of spines at high pCO_2 in
299 long term (>1 year) cultures of adult *Stylophorum pistillata* but Scucchia et al., (2021a) reported a
300 reduction in numbers of these features in short term (9 days) incubations of *Stylophorum pistillata*
301 larvae. Cross sections through individual trabeculae indicate they can contain multiple RADs which
302 formed as multiple spines on the skeletal surface, extended and became bonded together by the
303 deposition of TDs (see Figure 2e, Allison et al., 2001). It is unclear if the change in skeletal
304 morphology reflects an increase in the number of spines deposited or a reduction in the production
305 of thickening deposits that would normally obscure the spines inside the trabeculae.

306

307 **Origin of changes in skeletal morphology**

308   Increasing seawater pCO_2 can reduce the calcification rates of some corals but this does
309 not simply manifest as production of less skeleton of the same morphology as before but rather is
310 accompanied by significant changes in the skeletal structure. The deposition of $CaCO_3$ must be
311 precisely controlled to generate the highly organised and regular structures of coral skeletons
312 (Figure 1). This control likely occurs via enzymes and proteins which can promote and then inhibit
313 precipitation to control $CaCO_3$ nucleation, growth and shape. Skeletons of corals cultured at high
314 seawater pCO_2 have higher concentrations of skeletal organic material (Tambutte et al., 2015,

Coronado et al., 2019) and amino acids, the building blocks of the skeletal proteins (Kellock et al., 2020). The organic matrix extracted from tropical coral skeletons affects the precipitation of $CaCO_3$ *in vitro* (Falini et al., 2013) and is likely to play a role in the control of skeletal formation. At high pCO_2 *Stylophora pistillata* cell cultures (Drake et al. 2018) and larvae (Scucchia et al., 2021a) upregulate genes encoding for proteins of the skeletal organic matrix. This could be a mechanism to facilitate $CaCO_3$ precipitation (Drake et al. 2018) and thereby offset the reduction in seawater saturation state under ocean acidification that is likely to hamper calcification. Aspartic acid, the most abundant amino acid in the coral skeletal organic matrix (Cuif et al. 1999), inhibits aragonite precipitation at the concentrations inferred to occur at the coral calcification site (Kellock et al. 2020). The degree of inhibition is affect by the seawater saturation state suggesting that changes in the dissolved inorganic carbon chemistry of the calcification media could influence the effects of biomolecules. However aspartic acid predominantly occurs in peptides and proteins in the skeletal organic matrix and it is unclear how these molecules influence aragonite precipitation rate and structure. RADs represent organic-rich regions of the skeleton (Von Euw et al., 2017) and increases in the concentration of the organic matrix could alter the relative proportion of RADS and TDs deposited by the coral. For example, higher skeletal organic matrix concentrations may inhibit the precipitation of TDs. Skeletal surfaces became smoother at high seawater pCO_2 in *Stylophora pistillata* (Coronado et al., 2019) and this may reflect changes in the organic matrix of the skeleton. Further work is required to elucidate the role of skeletal organic macromolecules in biomineralisation at high seawater pCO_2.

It is intriguing to consider how different coral genotypes respond to ocean acidification. Genotype G7 was the fastest calcifying coral in the study (both at high and low seawater pCO_2, Cole et al., 2018, Figure 3c). However, at high seawater pCO_2 this genotype demonstrated the most pronounced decrease in trabeculae width, had prolific RADs and exhibited a disturbance in the regular placement of trabeculae and synapticulae, indicating that the biomineralisation process had been significantly impacted. This has parallels with culture studies which suggest that faster calcifying coral species demonstrate larger reductions in calcification in response to increased seawater pCO_2 than slow calcifying species (Comeau et al., 2014). The energetic costs of calcification, covering the extrusion of H^+ from the calcification site by Ca-ATPase (Al-Horani et al., 2003) and SOM synthesis (Allemand et al., 2011) are likely higher for faster calcifying individuals. These fast growing individuals may be unable to sustain their calcification energy budgets at high seawater pCO_2 and may be the least resilient individuals to ocean acidification.

system build and Truce Jack, Alex Millar and Innes Manders for assistance with preliminary image analysis. John Still assisted with scanning electron microscopy in the ACEMAC Facility at the University of Aberdeen.

Competing interests

Author contributions

All authors made substantial contributions to the conception or design of the work or the acquisition, analysis, or interpretation of the data. The first draft of the manuscript was written by Nicola Allison and all authors commented on previous versions of the manuscript. All authors read and approved the final manuscript.

Data availability

All data generated or analysed during this study are included in this published article as Appendix 2. Additional images of the coral skeletons are included in the supplementary data.

References

Al-Horani FA, Al-Moghrabi SM, de Beer D (2003) The mechanism of calcification and its relation to photosynthesis and respiration in the scleractinian coral *Galaxea fascicularis*. Marine Biology 142:419-426.

Allemand D, Tambutté É, Zoccola D, Tambutté S (2011) Coral calcification, cells to reefs Coral reefs: an ecosystem in transition. Springer, pp119-150.

Allison N, Cole C, Hintz C, Hintz K, Rae J & Finch A (2021), Resolving the interactions of ocean acidification and temperature on coral calcification media pH. Coral Reefs, https://doi.org/10.1007/s00338-021-02170-2.

Allison N, Finch AA, Sutton SR and Newville M (2001). Strontium heterogeneity and speciation in coral aragonite: implications for the strontium paleothermometer. Geochimica et Cosmochimica Acta, 65:2669-2676.

Barry JP, Tyrrell T, Hansson L, Plattner G-K and Gattuso J-P (2011) Atmospheric CO_2 targets for ocean acidification perturbation experiments. In Guide to best practices for ocean acidification research and data reporting (eds. U Riebesell, VJ Fabry, L Hansson and J-P Gattuso) European Communities, Belgium.

Chen PY (2015) Evaluating the economic damage of climate change on global coral reefs, Global Environmental Change, 30:12-20.

Chomsky O, Kamenir Y, Hyams M, Dubinsky Z, Chadwick-Furman NE (2004) Effects of temperature on growth rate and body size in the Mediterranean Sea anemone Actinia equina. Journal of Experimental Marine Biology and Ecology,313:63-73.

Cole C, Finch A, Hintz C, Hintz K, Allison N (2016) Understanding cold bias: Variable response of skeletal Sr/Ca to seawater pCO_2 in acclimated massive *Porites* corals. Scientific Reports 6.

Cole C, Finch A, Hintz C, Hintz K, Allison N (2018) Effects of seawater pCO 2 and temperature on calcification and productivity in the coral genus *Porites* spp.: an exploration of potential interaction mechanisms. Coral Reefs 37:471-481.

Comeau S, Edmunds PJ, Spindel NB, Carpenter RC (2014) Fast coral reef calcifiers are more sensitive to ocean acidification in short-term laboratory incubations, Limnology and Oceanography, 59:1081–1091.

Coronado I, Fine M, Bosellini FR (2019) Impact of ocean acidification on crystallographic vital effect of the coral skeleton. Nat Commun 10, 2896 (2019). https://doi.org/10.1038/s41467-019-10833-6.

397 Crook ED, Potts D, Rebolledo-Vieyra M, Hernandez L, Paytan A (2012) Calcifying coral abundance near
398 low-pH springs: implications for future ocean acidification. Coral Reefs 31:239-245.

399 Cuif JP, Dauphin Y and Gautret P (1999). Compositional diversity of soluble mineralizing matrices in some
400 recent coral skeletons compared to fine-scale growth structures of fibres: discussion of consequences for
401 biomineralization and diagenesis. International journal of earth sciences, 88:582-592.

402 Cuif JP and Dauphin Y, 2005. The two-step mode of growth in scleractinian coral skeletons from the
403 micrometre to the overall scale, Journal of Structural Biology, 150, 319-33.

404 Drake JL, Mass T, Stolarski J, Von Euw S, van de Schootbrugge B and Falkowski PG (2020). How corals
405 made rocks through the ages. Global change biology, 26:31-53.

406 Drake JL, Schaller MF, Mass T, Godfrey L, Fu A, Sherrell RM, Rosenthal Y and Falkowski PG (2018)
407 Molecular and geochemical perspectives on the influence of CO2 on calcification in coral cell
408 cultures. Limnology and Oceanography, 63:107-121.

409 Edmunds PJ (2012): Effect of pCO$_2$ on the growth, respiration, and photophysiology of massive *Porites* spp.
410 in Moorea, French Polynesia. Marine Biology, 159:2149-2160.

411 Elhadj S, De Yoreo JJ, Hoyer JR & Dove PM (2006) Role of molecular charge and hydrophilicity in regulating
412 the kinetics of crystal growth. Proc. Natl. Acad. Sci. U. S. A. 103: 19237–19242.

413 Erez J, Reynaud S, Silverman J, Schneider K, Allemand D (2011) Coral Calcification Under Ocean
414 Acidification and Global Change. In Coral reefs: an ecosystem in transition. Springer.

415 Fabricius KE, Langdon C, Uthicke S, Humphrey C, Noonan S, De'ath G, Okazaki R, Muehllehner N, Glas
416 MS, Lough JM (2011) Losers and winners in coral reefs acclimatized to elevated carbon dioxide
417 concentrations. Nature Climate Change 1:165-169.

418 Falini, G. *et al.* (2013) Control of aragonite deposition in colonial corals by intra-skeletal macromolecules. J.
419 Struct. Biol. 183:226–238.

420 Falini G, Fermani S, Goffredo S (2015) Coral biomineralization: A focus on intra-skeletal organic matrix and
421 calcification. Semin. Cell Dev. Biol. 46:17–26.

422 Foster T, Falter JL, McCulloch MT, Clode PL (2016). Ocean acidification causes structural deformities in
423 juvenile coral skeletons. Science advances. 2016 Feb 1;2(2):e1501130.

424 Herman A, Addadi L & Weiner S (1988) Interactions of sea-urchin skeleton macromolecules with growing
425 calcite crystals— a study of intracrystalline proteins. *Nature* 331, 546–548 https://doi.org/10.1038/331546a0.

426 Horvath KM, Castillo KD, Armstrong P, Westfield IT, Courtney T and Ries JB (2016) Next-century ocean
427 acidification and warming both reduce calcification rate, but only acidification alters skeletal morphology of
428 reef-building coral *Siderastrea siderea*. Scientific reports, 6:1-12.

429 Kellock C, Cole C, Penkman K, Evans, D, Kroger R, Hintz C, Hintz K, Finch A, Allison N (2020) The role of
430 aspartic acid in reducing coral calcification under ocean acidification conditions, Scientific Reports,
431 https://doi.org/10.1038/s41598-020-69556-0.

432 Kersting DK, Linares Prats C (2019) Living evidence of a fossil survival strategy raises hope for warming-
433 impacted corals. Science Advances, 2019, vol. 5, num. 10, p. eaax2950. 2019 Oct 9.

434 Kim YY, Carloni JD, Demarchi B, Sparks D, Reid DG, Kunitake ME, Tang CC, Duer MJ, Freeman CL,
435 Pokroy B and Penkman K (2016) Tuning hardness in calcite by incorporation of amino acids. Nature
436 materials, 15:903-910.

437 Kvitt H, Kramarsky-Winter E, Maor-Landaw K, Zandbank K, Kushmaro A, Rosenfeld H, Fine M, Tchernov D
438 (2015) Breakdown of coral colonial form under reduced pH conditions is initiated in polyps and mediated
439 through apoptosis. Proceedings of the National Academy of Sciences. 17:2082-6.

440 Lasker HR (1981) Phenotypic variation in the coral *Montastrea cavernosa* and its effects on colony
441 energetics. The Biological Bulletin.160:292-302.

442 McCulloch M, D'Olivo J, Falter J *et al.* (2017) Coral calcification in a changing World and the interactive
443 dynamics of pH and DIC upregulation. Nat Commun **8,** 15686. https://doi.org/10.1038/ncomms15686.

444 Mollica NR, Guo W, Cohen AL, Huang K-F, Foster GL, Donald HK, Solow AR (2018) Ocean acidification
445 affects coral growth by reducing density, Proc. Nat. Acad. Sci., 115 (8) 1754-1759; DOI:
446 10.1073/pnas.1712806115.

447 Scucchia F, Malik A, Zaslansky P, Putnam HM and Mass T (2021) Combined responses of primary coral
448 polyps and their algal endosymbionts to decreasing seawater pH. Proceedings of the Royal Society
449 B, 288:20210328.

450 Tambutté E, Venn AA, Holcomb M, Segonds N, Techer N, Zoccola D, Allemand D and Tambutté S (2015)
451 Morphological plasticity of the coral skeleton under CO_2-driven seawater acidification. Nature
452 communications, 6:1-9.

453 Ulstrup KE, Ralph PJ, Larkum AW, Kühl M (2006) Intra-colonial variability in light acclimation of
454 zooxanthellae in coral tissues of *Pocillopora damicornis*. Marine Biology. 149:1325-35.

455 Venn AA, Tambutte E, Holcomb M, Allemand D, Tambutte S (2011). Live tissue imaging shows reef corals
456 elevate pH under their calcifying tissue relative to seawater. PLoS ONE 6, e20013.

457 Venn AA, Tambutte E, Holcomb M, Tambutte S (2013) Impact of seawater acidification on pH at the tissue-
458 skeleton interface and calcification in reef corals. Proc. Natl. Acad. Sci. 110:1634-1639.

459 Von Euw S, Zhang Q, Manichev V, Murali N, Gross J, Feldman LC, Gustafsson T, Flach C, Mendelsohn R,
460 Falkowski PG (2017) Biological control of aragonite formation in stony corals. Science. 356:933-8.

461 Wells JW (1956) Scleractinia, in Treatise on Invertebrate Paleontology, Part F, Coelenterata, edited by R. C.
462 Moore, pp. 328 – 444, Univ. of Kansas Press, Lawrence.

463